REPORT NO. NADC 88067-60

AMBIENT TEMPERATURE PROPERTIES OF PM ALUMINUM — TITANIUM ALLOYS

William E. Frazier
Air Vehicle and Crew Systems Technology Department
NAVAL AIR DEVELOPMENT CENTER
Warminster, PA 18974

Michael J. Koczak
Drexel University
Department of Materials Engineering
Philadelphia, PA 19104

JUNE 1988

FINAL REPORT

Prepared for
NAVAL AIR DEVELOPMENT CENTER
Warminster, PA 18974

UNCLASSIFIED

SECURITY CLASSIFICATION OF THIS PAGE

ADA205997

REPORT DOCUMENTATION PAGE

Form Approved
OMB No 0704-0188

1a REPORT SECURITY CLASSIFICATION Unclassified	1b RESTRICTIVE MARKINGS
2a SECURITY CLASSIFICATION AUTHORITY	3 DISTRIBUTION/AVAILABILITY OF REPORT Approved for Public Release, Distribution is unlimited
2b DECLASSIFICATION/DOWNGRADING SCHEDULE	
4. PERFORMING ORGANIZATION REPORT NUMBER(S) NADC-88067-60	5 MONITORING ORGANIZATION REPORT NUMBER(S)
6a NAME OF PERFORMING ORGANIZATION Naval Air Dev. Center — 6b OFFICE SYMBOL (If applicable) 6063	7a NAME OF MONITORING ORGANIZATION
6c. ADDRESS (City, State, and ZIP Code) Warminster, PA 18974	7b ADDRESS (City, State, and ZIP Code)
8a NAME OF FUNDING/SPONSORING ORGANIZATION Naval Air Dev. Center — 8b OFFICE SYMBOL (If applicable) 6062	9 PROCUREMENT INSTRUMENT IDENTIFICATION NUMBER
8c. ADDRESS (City, State, and ZIP Code) Warminster, PA 18974	10 SOURCE OF FUNDING NUMBERS PROGRAM ELEMENT NO 62234N; PROJECT NO RS34A57; TASK NO 1; WORK UNIT ACCESSION NO 3P180

11 TITLE (Include Security Classification)

Ambient Temperature Properties of PM Aluminum - Titanium Alloys

12 PERSONAL AUTHOR(S)

William E. Frazier and Michael J. Koczak

13a TYPE OF REPORT	13b TIME COVERED	14 DATE OF REPORT (Year, Month, Day)	15 PAGE COUNT
Final	FROM ______ TO ______	June 1988	

16 SUPPLEMENTARY NOTATION

Aluminum, Aluminides, Orowan Hall-Petch, Modulus

17 COSATI CODES			18 SUBJECT TERMS (Continue on reverse if necessary and identify by block number)
FIELD	GROUP	SUB-GROUP	
11	06		
11	06.01		

19 ABSTRACT (Continue on reverse if necessary and identify by block number)

The structure and properties of dispersion strengthened aluminum 4 and 6 weight percent titanium powder alloys were investigated as candidate materials for high temperature performance. Alloy rod was extruded from vacuum hot pressed billets of helium gas atomized, mechanically alloyed, and atomized plus mechanically alloyed powder. Microstructure and mechanical properties were fully characterized to assess the effect of disperoids on alloy strength, ductility, notch toughness, and modulus. The alloys exhibited low density (2.8g/cm^3), high modulus (85 GPa), good ductility (12%), and strength equivalent to Al-Fe-Ce alloys, e.g., 120 MPa at 250-300°C.

20 DISTRIBUTION/AVAILABILITY OF ABSTRACT ☐ UNCLASSIFIED/UNLIMITED ☐ SAME AS RPT ☐ DTIC USERS	21 ABSTRACT SECURITY CLASSIFICATION Unclassified
22a NAME OF RESPONSIBLE INDIVIDUAL Dr. William E. Frazier	22b TELEPHONE (Include Area Code) 215-441-1301 — 22c OFFICE SYMBOL 6063

DD Form 1473, JUN 86 — Previous editions are obsolete — SECURITY CLASSIFICATION OF THIS PAGE

S/N 0102-LF-014-6603

UNCLASSIFIED

Table of Contents

LIST OF TABLES

LIST OF FIGURES

Introduction

Advanced powder metal (P/M) aluminum alloys are currently being developed using mechanical alloying and rapid solidification techniques. The objective it to obtain a homogeneous microstructure consisting of finely dispersed thermally stable compounds. To achieve this goal, aluminum is alloyed with elements having low diffusion rates and low solid state solubilities. Screening studies conducted by Sanders and Hildeman (1), Adams et al. (2) and Griffith et al. (3) laid the foundation for the development of the current generation of elevated temperature RST aluminum alloys based on transition elements, e.g., Fe, Mo, V, and Cr. These elements form high melting point aluminides which are resistant to deformation and coarsening.

Mechanically Alloying (MA) has also been used to produce aluminum alloys with excellent mechanical properties at potential service temperatures of 250-300°C. (4,5) These materials derive their elevated temperature properties from the fine dispersion of aluminides, carbides, and oxides distributed in their microstructures.

In the MA process, elemental powders are milled in the presence of a carbon bearing compound such as alcohol or stearic acid. During the process, the alloy powders are repeatedly fractured and cold welded. Cold welding is controlled by the amount and type of the carbon bearing process control agent used in the process. The oxide layer inherently present on the powder's surface is fracture upon impact. Oxides are dispersed into the materials along with the carbon bearing compound. New oxides regenerate on the fresh surface during the process. (6) The result is heavily cold worked powder of homogeneous composition and uniform of submicron oxides and carbides.

The oxides and carbides contribute to the strength of MA materials. Their fine size (0.01-0. 2μm) inhibits dislocation motion, prevents recrystallization, and curtails grain growth. Upon coarsening, they lose their effectiveness; consequently, the thermal stability of the carbides and oxides is important to the mechanical behavior of elevated temperature aluminum alloys. (7)

Aluminum - Titanium System:

Recent research indicated that the RST and mechanically alloyed Al-Ti alloys have good ambient and elevated temperature properties. (8, 9, 10) These alloys derive their mechanical properties from the fine dispersoids of Al_3Ti, Al_2O_3, and Al_4C_3 particles. The oxide and carbide dispersoids are products of the mechanical alloying process. The aluminide, Al_3Ti, can be formed by both primary solidification and peritectic transformation, Figure 1. (11). Additional Al_3Ti, 2-5 vol. %, may precipitate from the supersaturated aluminum matrix of rapidly solidified alloys.

A peritectic phase, transformation occurs at 665°C. and 1.15 wt.% (12) i.e., $L+\tau(Al_3Ti)$ - $\alpha(Al)$ The exact wt.% Ti contained in the first solid to form during the peritectic decomposition is reported to be between 1.15-1.3% (12, 13, 14). At the transformation temperature, titanium solubility in the liquid is 0.12 wt.%. Al_3Ti (13) has a body centered tetragonal structure, space group 14/mmm, 8 atoms/unit cell with a = 0.3851 nm and c = 0.86 nm.; density of 3370 kg/m^3. Fig. 1. (15) Precipitation of Al_3Ti from a supersaturated solid solution has been reported to result in an intermediate metastable semicoherent phase, Al_3Ti. This phase is believed to be similar to the cubic Al_3Zr' phase (13); and may belong to the space group $P6_3/mmc$.(16)

Strengthening Mechanisms;

The properties of aluminum alloys can be tailored for enhanced strength, toughness, and corrosion resistance. (17) By an empirical and theoretical understanding of the synergistic relationship between the

alloys' structure property and processing history, (18) aluminum alloys may be strengthened by a variety of means including solid solution strengthening, cold work, grain size, crystallographic texture, age hardening, and dispersion strengthening. This partial list of strengthening mechanisms has a common objective: To impede the motion of dislocations and thereby inhibit deformation and increase strength.

The ambient temperature strength of high temperature RST and mechanically alloyed alloys is typically achieved through a combination of mechanisms, i.e., dispersion strengthening, grain size, and texture: emphasis, therefore, will be placed on these strengthening mechanisms.

Crystallographic Texture: Crystallographic texture is developed during alloy processing. Since texture is the preferred orientation of crystallographic planes, its development affects both elastic and plastic response of the materials. The elastic modulus of single crystal aluminum varies from 76.1 GPa in the (111) direction to 63.7 GPa in the (100) direction. (19) The modulus of polycrystalline aluminum is seen to be dependent on the average orientation of the individual grains. Schmid (20) was the first to recognize that a critical resolved shear stress must be exceeded to produce slip in a single crystal along specific planes and directions, i.e., the ease of deformation was dependent on crystallographic orientation. Taylor (21) and, later, Bishop and Hill (22) developed a relationship between tensile yield stress, σ, and critically resolved shear stress, τ, for polycrystalline fcc and bcc materials.

$$\sigma = M\tau \qquad [1]$$

The average "Taylor Factor", M was estimated to be 3.1. The development of texture alters the Taylor factor and hence the alloy's strength. Palmer et al. (23) investigated the effect of texture on the tensile properties of extruded powder metallurgy alloy Al-3Li-2Cu-0.2Zr. The (111) pole intensity within 5 degrees of the tensile axis was measured and correlated to the alloy's yield strength. Yield strength was found to vary from 420 to 520 MPa as relative intensity of the (111) pole changed form 2 to 22.

Hall Petch Relationship: Hall (24) and Petch (25) developed a mathematical model (the Hall-Petch equation) relating yield stress, σ, to the grain size, L, of ferrous alloys. Where σ_0 and k_1 are materials constants. The Hall-Petch equation has since been found to be valid for most polycrystalline alloys and aluminum alloys. (26, 27)

$$\sigma = \sigma_0 + k_1 L^{-1/2} \qquad [2]$$

Wert (28), Kim and Griffith (29) have examined the effect of grain size on the yield stress of 7000 series (Al-Mg-Zn) aluminum alloys. The Hall-Petch slope, k_1, for peak aged 7075 was estimated at 120 MPa $\mu m^{1/2}$; and for underaged 7091 with grain size range 2.4 to 46 μm, the Hall-Petch slope was 220 MPa $\mu m^{1/2}$. Decker (26) presents yield strength and grain size data for an aluminum copper alloy and for commercially pure aluminum. The Hall-Petch slopes were calculated to be 125 MPa $\mu m^{1/2}$ and 75 MPa $\mu m^{1/2}$ respectively.

Orowan Strengthening: The hardening of metallic alloys by the utilization of second phase disperoids have been reviewed thoroughly several authors (17, 30, 26, and 31). The strength of an alloy containing a dispersion of incoherent impenetrable particles was first considered by Orowan. (32) The shear stress required for a dislocation to loop a particle was found to depend on the properties of the matrix and inversely upon the spacing of the particles.

Orowan's original relationship has been modified by a number of authors to account for the dislocation dipole effect, dislocation line tension, and the mean planar spacing of particles of finite diameters. (31) Dislocation dipole results when a dislocation bows around a defect. Dislocation of opposite sign come in close proximatey; consequently, the stress required for looping is reduced. A

further modification to the Orowan model was necessary to account for the fact that the line tension of edge dislocation is greater than that of a screw dislocation.

Also, the center to center spacing between large particles does not adequately describe the length of a dislocation bowing between these particles. This factor was accounted for by substituting the equation for mean planar spacing (i.e., the average distance between particle surfaces) for average particle spacing. This more precise version was derived by Martin (31) and presented below.

$$\tau = \frac{0.81Gb}{2\pi (1-\nu)^{1/2}} \frac{\ln (2r_s/r_0)}{(\lambda_s - 2r_s)} \quad [3]$$

Where G is the shear modulus of a aluminum; b is Burger's vector; r_0 is the dislocation core radius; ν is Poisson's ratio; λ_s is the average center to center spacing of particles; and r_s is the average radius of a particle. A plot of shear strength versus particle radius was generated using equation (3), Figure 2 and illustrates the requirement for fine particles and high volume particle fractions, e.g., radii $\leq$ 0.05 μm and volume fractions $\geq$ 0.1.

EXPERIMENTAL PROCEDURE

Materials Processing

Aluminum 4 and 6 wt.% titanium alloy powders were produced by inert gas atomization, mechanical alloying, and mechanical alloying the atomized powder alloys. The alloys were designated according the powder production technique used and the amount of titanium: AT for atomized, MA for mechanically alloyed, and AM for atomized and mechanically alloyed. An organic antiwelding agent (stearic acid) was added to the mechanically alloyed powders to introduce carbon into the system. The powders were degassed, vacuum hot pressed, and extruded into round rod. A flow chart of the processing sequence is presented in Figure 3.

Powder Production: Alloy powders were helium gas atomized and screened to -325 mesh (-44um) in a nitrogen/trace oxygen atmosphere by Valimet, Stockton, CA. The mechanically alloyed powder was produced by Novamet, Wyckoff, NJ. Alcan 99.9% pure aluminum was mechanically alloyed with pure titanium to create a master alloy with a chemistry of Al_3Ti. The master alloy was annealed for 24 hrs. at 1000°C in a vacuum in order to promote aluminide formation and homogenize the microstructure.

The annealed master alloy was then mechanically alloyed with pure aluminum. Two alloy powders were produced containing 4 and 6 wt.% Ti plus residual amounts of carbon, hydrogen, and oxygen from the 1 to 1.5 wt.% Stearic acid antiseizing agent.

Half of the inert gas atomized alloy powders were mechanically alloyed using similar processing conditions as the mechanically alloyed powders. This procedure serves to homogenize the microstructure and introduce carbon and oxygen to the system. During processing, one wt.% stearic acid was added to AM4 powder and 1.5 wt.% to AM6 powder.

Consolidation: The powder alloys were cold pressed into 10 Kg billets 0.15m in diameter and vacuum degassed at 427°C. The degassed billets were vacuum hot pressed at 493°C and 34 MPa. The billets were heated to a nominal temperature of 410°C, transferred to a container at 316°C and extruded (at an extrusion ratio of 47:1) into 22mm diameter rod through a cylindrical die with a cone angle of 30°.

MICROSTRUCTURAL CHARACTERIZATION

X-ray Diffraction: X-ray diffraction was used to identify the phases present in the powders and wrought alloys and to monitor the change in volume fraction of Al_3Ti resulting from thermal exposure. X-ray analysis was performed on a Rigaku DMAX-B x-ray unit equipped with a $\theta/2\theta$ goniometer and a graphite monochromator. X-rays were generated using a copper tube operating at 50KV and 20ma. The scan rate was 1°/min and data was collected every 0.04 degrees.

The preferred crystallographic orientation of the alloy rod was assessed using the Schulz reflection technique. The intensity of the peaks were recorded, analyzed, and plotted in the form of (111) and (200) pole figures.

Electron microscopy (SEM/TEM): An Amray scanning electron microscope equipped with a energy dispersive and wavelength dispersive x-ray spectrometer was operated at 20 Kv in the secondary electron emission mode. The SEM was used to characterize the fracture surfaces of the static mechanical test specimens. Thin foils of the materials were examined using a JOEL 100CX II transmission electron microscope operating at an accelerating voltage of 120kv. Samples were prepared for electropolishing by using a jeweler's saw to cut the rod into 0.6mm thick sections. Following hand grinding to 0.1mm, 3mm diameter disks were punched for electropolishing. Foils were prepared on a Struers twin jet electropolisher in a solution of 30% nitric acid and 70% methanol. The thinning conditions were 12v, 1.5ma, and a bath temperature of -30°C.

Image Analysis: The size and distribution of disperoids were characterized quantitatively by computer assisted techniques. The fine disperoid of aluminides, carbides, and oxides observed by TEM were measured manually. Particle diameters were calculated by averaging their length and breadth. A Cambridge Quantimet 970 was used in tandem with a high resolution video camera in order to analyze the microstructures of mounted and polished specimens observed by TEM. Particle diameters were calculated from the observed surface areas by assuming that the particles were spherical.

Mechanical Properties

Mechanical tests were performed on the consolidated alloys in order to evaluate their ambient temperature response. Tensile tests were conducted in accordance with ASTM E8-81 (33), on an Instron test machine, at a strain rate of 1.1×10^{-4} s^{-1}. The temsile specimens were 100mm long and 13mm in diameter. The reduced section was 37mm long and 6mm in diameter. Using a 25mm MTS extensometer, strain measurements were made in order to obtain Young's Modulus. In order to insure accuracy, 4 measurements per specimen were made at 90° intervals around each sample.

Notch tensile tests were performed using a modified tensile specimen having a notch with a root radius of less than 0.017mm (ASTM E602-81) machined in the mid-section of the sample.

Results and Observations

Microstructural Analysis of the Consolidated Alloy

Phase Identification: Phase identification of the alloys was accomplished by x-ray diffraction and selected area diffraction (SAD). There were four phases identified: fcc Al, bct Al_3Ti, hexagonal Al_4C_3, and cubic Al_2O_3. Al_4C_3 was found only in those alloys prepared from mechanically alloyed powder Very weak indications of the Al_2O_3 phase were found in all the alloys.

The second phase volume fractions were calculated based on compositional stoichiometry and are presented in Table I. Alloys AM6, MA4 and MA6 have 4.8 to 8.1 vol.% Al_4C_3; whereas, AM4 contains only 2.9 vol.% Al_4C_3. *the greatest amount of Al_2O_3 is present in the mechanically alloyed materials, e.g., 0.3 to 0.9 vol.% Al_2O_3. Alloys AT4 and AT6 contain approximately 0.2 vol.% Al_2O_3. The volume percent of Al_3Ti varies from 10.5 to 15.4 as titanium content increases from 4 to 6wt.%.

Table I.

Calculated Volume Percent
of Second Phases Based on Compositional Stoichiometry

ALLOY	Al_3Ti	Al_4C_3	Al_2O_3	TOTAL
AT6	15.01	0.06	0.24	15.31
AT4	14.30	0.05	0.18	14.53
AM6	15.39	4.76	0.28	20.43
AM4	12.66	2.92	0.86	16.44
MA6	12.58	8.05	0.89	21.51
MA4	10.52	5.83	0.54	16.90

Optical Microscopy: The microstructures of the extruded AT, AM, and MA alloys are presented in Figure 4. The microstructures of alloys AT4 and AT6 are similar consisting of homogeneously distributed Al_3Ti particles ranging in size from less than a micron to 15µm or more in diameter. The microstructural features of the AM alloys resolvable by optical techniques are identical to those of the AT materials, Figures 4a & b. In contrast, the microstructures of the MA alloys, Figure 4c, are distinct from those of either the AT or AM materials. In the MA alloys, ellipsoidal Al_3Ti particles 3 to 15µm in size are dispersed throughout the aluminum matrix; however, the finer 1µm size disperoids present in the AT and AM alloys are absent.

Transmission Electron Microscopy (TEM): TEM examination of the extruded powder alloys was conducted before and after exposing the alloys for 100 hrs. to temperatures up to 400°C. Figure 5 shows the microstructure of the as-received AT, AM, and MA alloys. The microstructures of the alloys annealed at 300°C for 100 hours are presented on Figure 6. Two morphologies of Al_3Ti particles are readily visible, i.e. spherical and grain-like. The grain-like morphology of Al_3Ti can be observed in alloy AM6, Figure 5a. A butterfly shaped, 0.2-0 4µm sized Al_3Ti pa. ticle is located in the upper left corner of Figure 6b.

The size distribution of Al_3Ti particles in the alloys AT, AM, and MA before and after isochronal annealing were measured and ranged in size from 0.01 to 0.5µm. Prior to thermal exposure, the average particle diameter is 0.08µm; after annealing for 100 hours at 300°C, the average particle diameter increases to 0.11µm. The distribution of particles in the 0.01 to 0.15µm size range appears relatively unaffected by annealing. However, the number of particles counted in the 0.20 to 0.50µm size range increases noticeably.

The finer dispersoids observed principally in alloys AM and MA; and located primarily at grain boundaries have been identified as $Al_4C_3$and Al_2O_3. The average size of these particles is estimated to be 0.01µm. The average grain size lies between 0.3 and 0.5µm and appears to be unaffected by the 100 hour long thermal exposure or 300°C.

Alloy Texture: Alloy texture, random intensity times peak intensity, for the (111) and (200) poles is presented in Table II. The alloy rods all exhibit the (111) fiber texture typical of extruded aluminum

alloys. However, alloys AT4 and AT6 have substantially higher pole intensities than do the AM or MA materials, e.g., the (111) pole intensity for AT4 is 16 and for MA4 is 5.

Table II

Texture of the Extruded Rod, Random Intensity Times Peak intensity for the (111) and (200) Poles.

Pole	AT6	AT4	AM6	AM4	MA6	MA4
(111)	22.2	15.8	4.2	10.3	2.8	5.2
(200)	3.7	2.8	1.9	2.3	1.6	1.7

Tensile Properties The temsile properties of the as-received extruded aluminum-titanium alloys are shown in Table III. Mechanical property results are the average of 2-3 tests and demonstrated little property variability, i.e., the standard deviation corresponding to yield strength, tensile strength, and modulus variation ranged from 0 to 4%. The yield strengths of the as-received AM and MA alloys range from 288 to 325 MPa and is about 140 MPa greater than the YS of the AT materials, e.g., AT6 180 MPa. The ultimate tensile strengths of the mechanically alloyed materials, MA4, MA6, AM4, and MA6, range from 321 to 351 MPa; whereas, the UTS of alloys AT4 and AT6 are 230 and 220 MPa.

Table III.

Ambient Temperature Tensile Properties

ALLOY	TENSILE STRENGTH (MPa)	YIELD STRENGTH (MPa)	PERCENT ELONGATION	PERCENT REDUCTION IN AREA	YOUNG'S MODULUS (GPa)	NT/UTS
AM6	351.3	320.9	9.0	12.5	86.7	1.2
AM4	320.9	287.7	15.0	29.8	85.7	1.5
AM6	347.1	325.1	8.0	20.6	80.3	1.4
MA4	338.1	318.3	9.3	27.1	73.9	1.4
AT6	220.4	180.4	21.0	33.4	88.2	1.5
AT4	229.6	177.8	22.0	41.1	91.1	1.5

The alloy work hardening, i.e., the difference between an alloys's UTS and YS, is listed by alloy in descending order of their ability to work harden: AT4, AT6, AM4, AM6, MA6, and MA4. The difference between the UTS and YS of alloy AT4 is 50 MPa, but reduces to 20 MPa for MA4. The difficulty of the PM aluminum-titanium alloys is inversely related to their YS. The materials with the lowest YS, AT4 and AT6, have tensile elongations of 21 to 22%. The elongation of the strongest three alloys, MA4, MA6, and AM6, is 8 to 9% and the elongation of alloy AM4 is 15%.

The average Young's Modulus of the alloys (84.4GPa) is 21% greater than that of conventional high strength aluminum (70GPa). The moduli of the AT and AM alloys range from 86 to 91 GPa and is significantly greater than that of the MA alloys, e.g., 74 GPa and 80 GPa for MA4 and MA6, respectively. Results of the notch tensile tests indicate that the alloys are not notch sensitive and implies good toughness. The NT/UTS values range form 1.25 to 1.5. Alloys AT4, AT6, and AM4 have the highest NT/UTS values, i.e. 1.5 and alloy AM6 the lowest at 1.25.

Fracture Behavior: Scanning electron microscopy (SEM) was used to examine the microstructures and fracture surfaces of AT, AM, and MA tensile specimens, are Figure 7. Macroscopically, all the tensile fracture surfaces examined had the cup and cone appearance typical of ductile tensile failures.

AT4 has a dimpled fracture surface. The dimples range in size from less than 0.05μm to greater than 3.0μm, Figure 7a. Similarly, AM4 has a fine dimpled fracture surface. However, the dimples are smaller and more homogeneously distributed. The dimples range in size from 0.5 to 1.0μm, Figure 7b. MA4 has large (0.5 by 4.0μm) rectangularly shaped holes dispersed throughout a fine (0.2 to 1.01μm) and homogeneously dimpled fracture surface, Figure 7c. The large holes are most likely the result of plates of Al_3Ti pulling away from the matrix fracture.

Discussion of Results

Microstructure of the Extruded Rod

Optical Metallography: The optical micrographs of the AT and AM alloys are similar in appearance, Figure 4a & b. Particles range in size from 1 to 15μm and are homogeneously distributed throughout the aluminumatrix. Unfortunately, the details of the grain structure can nor be readily observed optically. In contrast, the microstructure of the MA alloys are relatively coarse and inhomogeneous, Figure 4c. The particles range in size from 3 to 15μm and are inhomogeneously distributed throughout the alloy's microstructure, Table IV.

However, despite the obvious microstructural differences between the AM and MA alloys their mechanical behavior are similar and distinct from the AT materials. This observation leads to the conclusion that the microstructural features controlling mechanical behavior are optically unresolvable.

Phase Identification: X-ray diffraction of the as-received alloys confirmed the presence of bct Al_3Ti but was unable to detect $Al_{24}Ti_8$, Al_4C_3, and Al_2O_3. Selected area diffraction (SAD) established the presence of Al_4C_3 and Al_2O_3 in the microstructures of the mechanically alloyed materials. Ring, not spot patterns were seen for Al_4C_3 phase even when the smallest diffraction aperture was used and this indicated a high volume fraction of fine (0.01μm) Al_4C_3 disperoids having no preferential habit plane relative to aluminum.

No other phases were identified. This may appear surprising considering that the major alloying element is titanium and titanium is known to react strongly with carbon and oxygen. Koczak et al. (34) have demonstrated that TiC can be produced by melting these alloys in the presence of carbon. Recently however, Banerji and Reif (35) evaluated the thermodynamic stability of TiC in the presence of Al_4C_3 and concluded that Al_4C_3 was the stable phases at temperatures below 1000°C. Furthermore, TiO_2 does not form even though its free energy of formation is low (-178kcal at 600°C) because Al_2C_3 is even more stable, i.e., -222kcal at 600°C. This thermodynamic stability holds over the entire temperature range of their existence.

Grain Size and Particle Distribution: The grain size and Al_3Ti particle size distributions for the AT, AM, and MA alloys are presented in Table IV. The average grain size of the as-received materials was measured to be 0.4μm. Although the angular relationship between grains was never actually measured, it is believed that they are high angle boundaries based primarily on TEM observation of their microstructures and SAD patterns.

Table IV
Alloy Grain Sizes and Fine Particle Sizes

Alloy	Grain Size, μm	Particle Size, μm
AT6	0.74	0.13
AT4	0.47	0.07
AM6	0.29	0.04
AM4	0.31	0.08
MA6	0.32	0.05
MA4	0.28	0.05

The average Al_3Ti particle size for the aluminum-titanium alloys was 0.08μm using TEM and 0.7μm using SEM. The larger plate-like particles, e.g., 1-40μm are the result of primary solidification of Al_3Ti and may be the result of atomization below the alloy's liquidus temperature. This particle morphology has been reported in the solidified microstructure of aluminum-titanium alloys by numerous investigators. (36-39) The fine spherical particles are the result of solid state nucleation and growth during processing.

Microstructural Model: In order to more fully appreciate how the various features interact, an idealized model was developed. The model is based upon the average grain size and particle size data collected from optical, SEM and TEM techniques. The model accurately represents both the average size and spacing of microstructural features but does not account for feature shape, size variation and volume fraction.

Figure 8 is a graphical representation of the microstructural model. The right side represents the microstructure of the AM and MA alloys containing Al_4C_3. The other side represents the microstructure of the AT materials. Examination of the figure 8 reveals that there are Al_3Ti particles on the order of the grain sizes, i.e., 0.4μm and spaced about 1μm apart. The spherical Al_3Ti particles o.1μm in diameter are preferentially located along the grain boundaries and have a spacing of 0.2 to 0.7μm.

The fine Al_4C_3 and Al_2O_3 particles present in the AM and MA alloys are also preferentially located at grain boundaries. These particles are 0.01μm in diameter and spaced about 0.04μm apart. In the next section, the mechanical properties of the alloys will be discussed in light of this microstructural model.

Discussion of Mechanical Properties:

Tensile Strength: In this section, an attempt is made to establish what relationship exists between microstructure and tensile strength and to correlate tensile test results to the various accepted strengthening models. However, difficulties arise when attempting to describe alloy strength based on the complex microstructures found in these P/M aluminum titanium alloys. As described in the previous section, the microstructure consists of four phases present in a variety of morphologies, sizes, and volume fractions. This implies that the alloys' response could be a combination of what is typically found in dispersion strengthened, particle strengthened, or two phase aggregates composite materials.

Both shearable and nonshearable particle strengthening mechanisms were considered; however, models based on shearable particles were eliminated early in the analysis because of several factors: (1) no evidence of particle -matrix coherency was found, (2) no evidence of sheared particles as found, and (3) significant strengthening is predicted only for extremely fine particles and large volume fractions e.g., particle diameters much less than 0.01μm and volume fractions greater than 0.10.

Orowan strengthening, eq. (3), by dislocation looping of disperoids was calculated using particle size data collected during image analysis. The results for the dispersion of Al_3Ti and Al_4C_3 are illustrated graphically in Figure 9. As can be seen from Figure 9, Al_3Ti contributes little to the alloys' strength and cannot be used to explain the differences in properties between the various materials.

In contrast to the results for the strengthening affect of Al_3Ti, a strong correlation was found to exist between the presence of Al_4C_3 and alloy strength, Figures 9 and 10. However, the predicted strength is two to three times as great as was actually measured. This may be the result of the microstructural inhomogeneities. Particles are distributed at the grain boundaries and may indicate that the Orowan strengthening model is not strictly applicable.

Despite the small effect of grain size on conventional aluminum alloys' strength, it was investigated as a possible strengthening mechanism. Alloy strength plotted against the inverse square root of grain size was found to form a straight line as predicted by the Hall-Petch model. The Hall-Petch slope was calculated to be 165 PMa$(\mu m)^{0.5}$. This is in excellent agreement with the value reported in the literature for conventional aluminum alloys, e.g., for Al-Mg-Zn alloys: 120-220 MPa$(\mu m)^{0.5}$ (40) and for Al-Cu alloys 75-125 MPa$(\mu m)^{0.5}$. (26)

The alloys' strength is then seen to be strongly related to grain size and Al_4C_3 disperoids but weakly to the presence of Al_3Ti. By examining the microstructural model presented earlier in Figure 8, the spacing of the large and small aluminides are seen to be of the same dimension as the grain size; consequently, it is unlikely that mechanism involving dislocation bowing around the aluminides contribute to the alloy's strength significantly. Futhermore, since the carbides and oxides are concentrated at the grain boundaries, it is likely that Orowan type calculations which assume a homogeneous distribution of particles would overestimate their strengthening effect.

Therefore, it is concluded that the primary effect of the disperoids is to inhibit grain growth and maintain strength via the Hall-Petch mechanism. The inhibition of grain growth by second phase particles can be estimated using Zener Relationship.

$$L = 1.33C_z(r/f) \tag{4}$$

Where C_z is Zener's constant; r is particle radius; f is volume fraction of particles. The fine size of the carbides and aluminudes make them effective in controlling grain growth in the MA and AM materials. In the absence of carbides in the AT alloys the aluminides, which are in order of magnitude greater in size, must control grain size.

The strength of the mechanically alloyed materials, AM and MA, is 100 to 120 MPa greater than that of the rod produced from the prealloyed powders, Table III and V. This can be related directly to the presence of the fine carbides and oxides present in their microstructure. However, no relationship was found to exist between strength and the volume fraction of Al_3Ti particulates.

Ductility: The helium gas atomized alloys (AT) exhibited the best ductility: 21-22% elongations and 33-41% reduction in area, Table V. The AM and MA materials had elongations of 8-12% and reduction in areas of 20-29%. The reduced ductility of the AM and MA alloys is directly associated with the presence of the fine aluminum carbide and aluminum oxide particles which decorate the grain boundaries. This assertion is supported by the fact that the AT materials which exhibit good ductility are essentially carbide free. Also, alloy AM4 has half the carbon content and nearly twice the ductility of the other AM and MA alloys, Table VI.

TABLE V.

Tensile Properties of the Annealed Rod

ANNEAL TEMP. (°C)	ALLOY	TENSILE STRENGTH (MPa)	YIELD STRENGTH (MPa)	PERCENT ELONGATION	PERCENT REDUCTION IN AREA
25	AM6	351.29	320.86	9.00	12.47
	AM4	320.92	287.66	15.00	29.77
	MA6	347.14	325.15	8.00	20.55
	MA4	338.07	318.30	9.33	27.07
	AT6	220.41	180.41	21.00	33.35
	AT4	229.56	177.82	22.00	41.10
200	AM6	352.45	329.52	9.00	16.87
	AM4	318.03	293.03	13.50	26.50
	MA6	361.83	345.03	6.50	15.75
	MA4	340.28	324.76	8.00	25.90
	AT6	228.69	178.93	16.00	21.35
	AT4	225.79	211.69	2.00	5.75
300	AM6	371.38	347.03	8.50	14.35
	AM4	340.28	315.76	15.00	26.70
	MA6	370.14	352.52	7.00	19.40
	MA4	361.24	349.48	7.50	17.45
	AT6	250.55	190.93	11.50	16.45
	AT4	212.00	183.00	23.00	40.70
400	AM6	349.07	327.55	8.50	15.05
	AM4	330.14	303.17	13.00	23.50
	MA6	361.24	342.31	5.00	12.50
	MA4	338.24	324.69	8.00	19.75
	AT6	219.79	170.79	14.50	21.15
	AT4	215.38	158.21	21.00	38.80
500	AM6	349.03	312.21	7.00	10.25
	AM4	317.97	312.21	7.00	10.25
	MA6	307.83	289.28	2.00	2.30
	MA4	301.86	281.45	4.00	5.30
	AT6	201.10	151.34	16.00	30.95
	AT4	198.07	134.28	24.00	46.50

Table VI.
Composition of the Powder Alloys (Weight percent)

Materials	Ti	C	O
AT4	4.04	0.01	0.12
AT6	5.89	0.01	0.16
MA4	4.70	1.25	0.37
MA6	5.60	1.72	0.60
AM4	5.60	0.62	0.58
AM6	6.32	1.01	0.19

Notch Tensile Strength: The PM aluminum-titanium alloys all exhibit excellent notch tensile strengths as indicated by the NT/UTS ratios given in Table III. The NT/UTS ratios range from 1.25 to 1.5. Values less than one are associated with alloys that are notch sensitive and values greater than one indicated good toughness in high strength aluminum alloys.

The presence of a sharp notch in the gage section of the test sample as a stress concentration creating a complex triaxial stress below the root of the notch. Evoking wither the Tresca or Von Mises criteria for the onset of yielding indicated onset of plasticity is suppressed to higher axial stress levels. Corresponding to the increase in strength is an increase in the hydrostatic component of stress. Alloys exhibiting poor matrix particle bonding would tend to fail at the interface under such hydrostatic stresses. Likewise, microvoid coalescence at the interface of any variety of microstructural features eventually leads to failure.

The high levels of NT/UTS can than be attributed to good matrix particle bonding, a ductile aluminum grain and a fine (0.5µm) grain size. The homogeneous grain structure helps to distribute the stress evenly and the ductile aluminum grain interior is able to accommodate local strain incompatibilities at the particle matrix interfaces.

Elastic Modulus: The modulus of conventional aluminum alloys is generally considered to be insensitive to microstructure, composition and processing history. However, it is known that the development of preferred crystallographic orientation, e.g., texture, the presence of second phases, and the addition of certain alloying elements can affect elastic modulus.

The results of the microstructural and crystallographic investigation of aluminum titanium alloys studied suggest that a complex synergistic relationship exists between modulus, texture, particles and composition. Young's modulus is observed to increase from 80 to 90 GPa as the intensity of the (111) pole increased from 2 to 22, Figure 11. Modulus also increases from 75 to 90 GPa as the volume percent of Al_3Ti is increased from 10.5 to 15, Figure 12. Although, no correlation was observed between modulus and the volume percent of Al_4C_3 and Al_2O_3. The development of texture, however, is curtailed by the presence of second phase particles. Figure 13 illustrated how the presence of Al_4C_3 reduces the amount of preferred orientation: similar correlations can be made for both Al_2O_3 and Al_3Ti.

The modulus of the Al_3Ti phase was calculated via the rule if mixtures using the mean value for particle volume fraction and alloy modulus; the modulus of aluminum matrix was assumed to 70 GPa. The modulus of the aluminide was computed to be 177.6 GPa and reflects a 2.5 GPa increase in the alloy's modulus for each wt.% Ti. This value agrees well with Mondolofo who reports a 2.6 GPa increase per wt.% Ti.(13) Although the modulus values for Al_3Ti are not available in the literature, Holowach and Redder (41) measured the moduli of Ti_3Al and AlTi to be 144.8 and 175.9 GPa respectively. Based upon the above discussion, 177.6 GPa appears to be reasonable value for the modulus of Al_3Ti.

Hall Petch and Orowan Strengthening

The strength of the PM aluminum-titanium alloys is primarily derived form their fine (0.5μm) grain size. The fine grain size is the result of the 0.01 to 0.1μm diameter dispersion of aluminides, carbides, and oxides preferentially located at the grain boundaries. Disperoids within the grain also enhance strength by impeding dislocation motion and improve ductility by providing a continuous source of dislocations.

Figure 14 is a plot of log yield strength versus log grain size for the aluminum-titanium alloys and commercially pure aluminum was cold rolled 70% and recovery annealed to achieve the strengths and grains size indicated (42). The linear nature of the plot indicates that grain boundary strengthening is operative.

Yield strength versus inverse square root grain size is plotted in Figure 15. The differences between the extrapolated values of aluminum and the PM aluminum-titanium alloys can result from numerous secondary strengthening effects, e.g., (a) the relative number of high to low angle grain boundaries, (b) Orowan strengthening, and (c) the increased mean matrix stress due to the presence of particles. In summary, the ambient temperature properties are the result of (i) Hall-Petch strengthening and (ii) Orowan strengthening by oxides and carbides with little effect from aluminides.

The Role of Oxides, Carbides and Aluminides

The variety of particle sizes, types, and volume fractions make it extremely difficult to isolate the individual contribution of a disperoid to an alloy's overall strength and creep properties. However, unambiguously the primary effect of the particles is to prevent grain growth beyond that predicted by Zener's relationship, i.e., equation (4). Zener's relationship predicts that the maximum grain size is proportional to particle radius and inversely proportional to particle volume fraction. Consequently, fine disperoids present in high volume fractions have the most significant impact on grain size.

Al_4C_3 plays a major role in the strengthening of the aluminum-titanium alloys because of its fine size, e.g., 0.01μm and high volume fractions, i.e., 0.03 to 0.08. Al_2O_3 particle have the same size as Al_4C_3 but have very low volume fractions and therefore alter alloy properties less dramatically. Al_3Ti is present in volume fractions ranging between 0.1 to 0.15; however, its means particle diameter is 100 times greater than that of Al_4C_3 and Al_2O_3. Consequently, the strengthening effect of Al_3Ti is only apparent in the carbon free alloy, e.g., AT6 and AT4. From Figure 15, the strength increase is estimated at 20-60 MPa.

Conclusions

1. The microstructure of the as-received extruded helium gas atomized powder alloys contains three phases, i.e., fcc Al, bct Al_3Ti, and cubic Al_2O_3.

2. Four phases were identified in the extruded Am and MA microstructures, i.e., fcc Al, bct Al_3Ti, cubic Al_2O_3, and hexagonal Al_4C_3.

3. The aluminide distribution of the AT and AM alloys is finer and more homogeneous than that of the MA materials.

4. Alloy grain size and texture is controlled by the fine distribution of aluminide, oxide, and carbide particles.

5. The Orowan Strengthening model is not strictly applicable to these alloy systems because: a) fine disperoids are inhomogeneously distributed, and b) the mean planar spacing of Al_3Ti particles is comparable to the grain.

6. Alloy strength can be explained in terms of the Hall-Petch relationship.

7. Annealing the aluminum-titanium alloys at 300°C for 100 hrs. increases strength. The increase in strength is attributable to the precipitation of Al_3Ti and the formation of Al_4C_3 and Al_2O_3.

8. Annealing at temperatures above 300°C reduces alloy strength and is attributable to Al_4C_3 and Al_2O_3 coarsening and grain growth.

References

1. R.E. Sanders, Jr, and G.H. Hildeman, "Elevated Temperature Aluminum Alloy Development," Final Report, AFWAL Contract No. F-3315-77-C-5086, (June, 1981).

2. C.M. Adam, R.G. Bourdeau, J.W. Broch, and A.R.COX, "Application of Rapidly Solidified Alloys," Final Report, AFWAL Contract No. F-33615-76-C-5136, (Dec, 1981).

3. "Elevated Temperature Aluminum Alloys for Aerospace Applications," High Strength Powder Metallurgy Aluminum Alloys. ed. M.J. Koczak and G.J. Hildeman. (Warrendale, PA: The Metallurgical Society, 1982),3

4. F.H Froes and J.R. Pickens, "Powder Metallurgy of Light Metal Alloys for Demanding Applications," Journal of Metals. (1984).

5. D.L Erich, "Development of a Mechanically Alloyed Aluminum Alloy for 450-650°F. Service," AFML-TR-79-4210, (August, 1979).

6. R.D. Schelleng and S.J. Donachie, "Mechanically Alloyed Aluminum," Metal Powder Report, 38, (10) (1983).

7. S.K. Kang, D.L. Erich, and H.F. Merrick, " The Mechanical Behavior of Mechanically Alloyed Al Alloys," ibid. ref. 3, p.317.

8. Heinz G.F. Wisdorf et. al., "Very High Temperature Aluminum Materials Concepts," Biannual report No. 2, AFWAL Contract No. F33615-86-C-5074, Light Metals Center, University of Virginia, (1987).

9. W.E. Frazier, "A Fundamental Study of the Mechanical and Microstructural Response of Elevated Temperature PM Aluminum-Titanium Alloys," (Ph.D. thesis, Drexel University, 1987).

10. G.S. Murty, M.J. Koczak, and W.E. Frazier, "High Temperature Deformation of Rapid Solidification Process/Mechanically Alloyed Al-Ti Alloys," Scripta Met. 21 (2) (Feb. 1987), 141-146.

11. Hultgren et. al.; Selected Values of the Thermodynamic Properties of Binary Alloys (Metals Park, OH: ASM, 1973).

12. D.H. St. John and LO.M. Hogan, "Thermal Stability in the Al-Al_3Ti System," Journal of Material Science, 15, (1980), 2369.

13. L.F. Mondolfo, Aluminum alloys: Structure and Engineering Materials. (NY, NY: John Wiley, 1976), 14.

14. M. Hansen, Constitution of Binary Alloys. (NY, NY: McGraw-Hill, 1958).

15. J.H. Westbrook, Ed. Intermetallic Compounds. (NY, NY: John Wiley and Sons, 1938), 307.

16. P. Villars and L.D. Calvert, Pearson's Handbook of Crystallographic Data for Intermetallic Phases. (Metals Park, OH: ASM, 1985), 1076.

17. E.A. Starke, Jr., "Aluminum Alloys of the 70's: Scientific Solutions to Engineering Problems. An Invited Review, "Materials Science and Engineering, 29, (1977).

18. R.J. Bucci, "Selecting Aluminum Alloys to Resist Failure by Fracture Mechanisms," Engineering Fracture Mechanics. 12, (Pergamon Press, 1979), 407-441.

19. R.W. Hertzberg, Deformation and Fracture Mechanics of Engineering Materials. (New York, NY: John Wilery, 1976) 14.

20. E. Schnid, Z. Electorochem, 37, (1931), 447.

21. G.J. Taylor, Journal Institute of Metallurgy, 62, (1938), 307.

22. J.F.W. Bishop and R. Hill, Phil. Mag., 42, (1951),414-427, 1928-1307.

23. I.G. Palmer, R.E. Lewis, and D.D. Crooks, "The Design and Mechanical Properties of Rapidly Solidified Al-Li-Y Alloys," Conf. Proc. AIME Aluminum Lithium Alloys. ed. T.H. Sanders, Jr. and E.A. Starke, Jr. May, 1980.

24. E.O. Hall, Proceedings of the Physics Society of London. 643, (1951), 747.

25. N.J. Petch, London Journal of Iron and Steel Industry, 173, (1953), 1145-1159.

26. R.F. Decker, Alloy Design Using Second Phases, "Met. Trans., 4, (Nov., 1973), 2495.

27. N. Hansen, "Effect of Grain Size on the Mechanical Properties of Dispersion-Strengthened Aluminum-Oxide Products," Transaction of the Metallurgical Society of the AIME, 245, (June, 1969), 1305.

28. J.A Wert, Strength of Metal Alloys, ed. R.C. Gifkins, (pergamon Press, 1980), 339.

29. Y.W. Kim and W.M. Griffith, PM Aerospace Materials, 1, (Shrewsburg, UK: MPR, 1984).

30. "The Strengthening Mechanisms of Aluminum Powder Alloys," AIME Conf. Proc. High Strength Powder Metallurgy Aluminum Alloys II. ed. G.J. Hildeman and M.J. Koczak, (Oct., 1985), 3.

31. J.W. Martin, Micromechanisms in Particle Hardened Alloys, (Cambridge, Cambridge University Press: 1980).

32. E. Orowan, in Symposium on Internal Stress in Metals and Alloys. (London: Institute of Metals, 1948), 451.

33. 1981 Annual Book of ASTM Standards. 10, (Phila., PA: American Society for Testing and Materials, 1981).

34. M.J. Koczak, M.K. Premkumar, and W.E. Frazier, In-situ Metal Matrix Comp Matrix Composites, "Presented at the Annual meeting of the American Ceramics Society/National Aeronautic and Space Administrations, Cocoa Beach Fl. Jan. 1986.

35. A. Banerji and W. Reif, "Development of Al-Ti-C Grain Refiners Containi Refiners Containing TiC," Metallurgical Transactions. vol. 17A, December 1986.

36. D.H. St. John, and L.M. Hogan, "Metallography and Growth Crystallography of Al_3Ti in Al-Ti Solid Solution Alloys, "Journal of Crystal Growth, 46, (1979), 585-587.

37. D.H. St. John, and L.M. Hogan, "Segregation Patterns in Unidirectionally Solidified Al-Ti Solid Solution Alloys, "Journal of Crystal Growth, 46, (1979), 585-587.

38. H. E1-Halfaway et. al., Al_3Ti Precipitates in a Chill-Cast *al-14wt.% Ti Alloy, "Metallography, 12, (9) (Sept., 1979).

39. J. Cisse,H.W. Kerr, and G.F. Bolling, "The Nucleation and Solidification Al-Ti Alloys, "Met. Trans., 5, (March 1974), 633.

40. U.V. Deshmukh, "Mechanical Properties and Microstructures of Manganese Modified Al-Zn-Mg-Cu P/M Aluminum Alloys," (Ph.D. Thesis, Drexel University, 1987).

41. J. Holowach and T.K. Redder, "Ti/Al Design/Cost Trade-Off Analysis," General Electric Co. for the Air Force Aero Propulsion Laboratory, Report No. AFAPL-TR-78-74, (Feb, 1979).

42. M. Sahoo and J.A. Lund, "Substructure and Dispersion Hardening in Aged Cold Worked, and Annealed Al-4Wt Pct Cu Alloy, "Met. Trans., 4, (January 1973). 39.

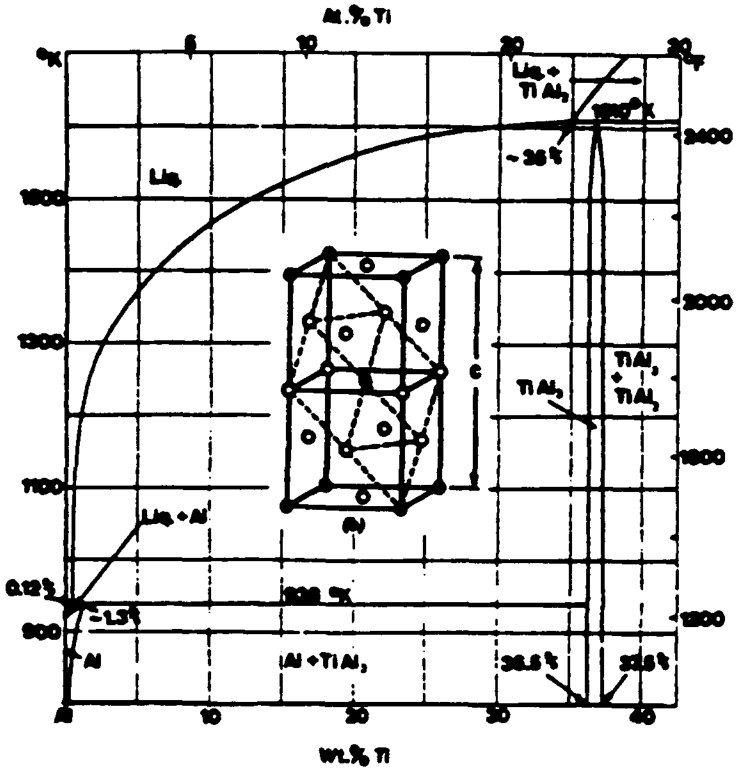

Fig. 1 Aluminum-Titanium Phase Diagram and the Crystal Structure of Al_3Ti.

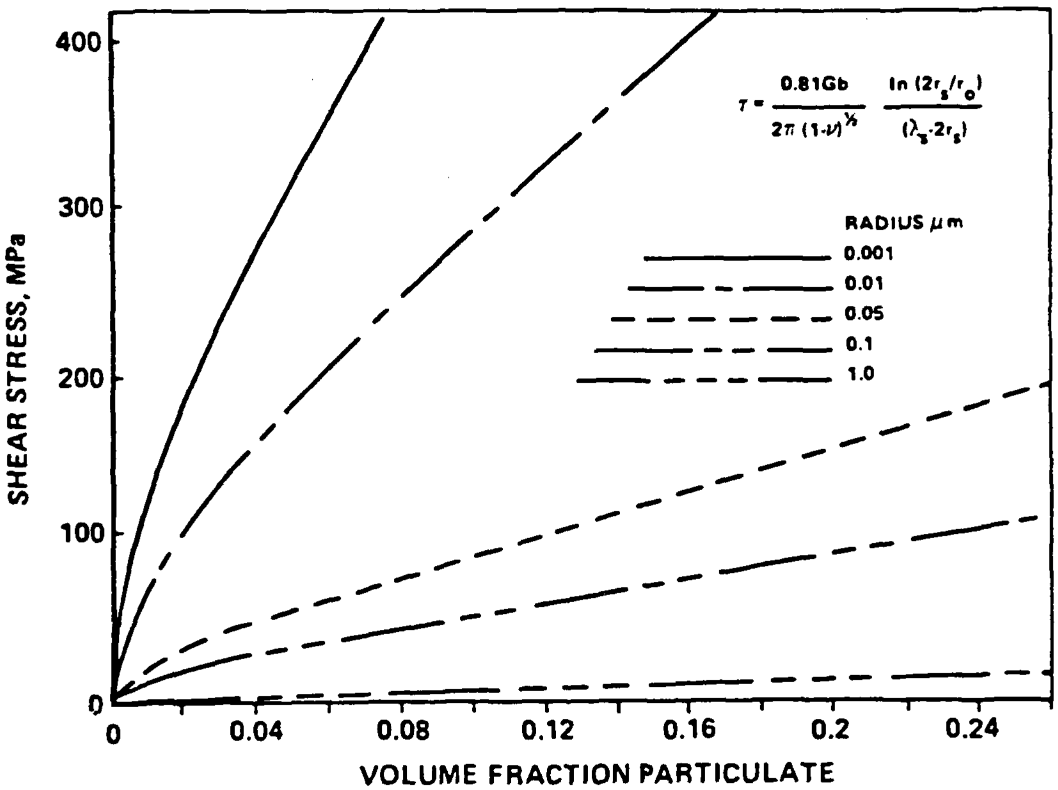

Fig. 2 Orowan Strengthening.

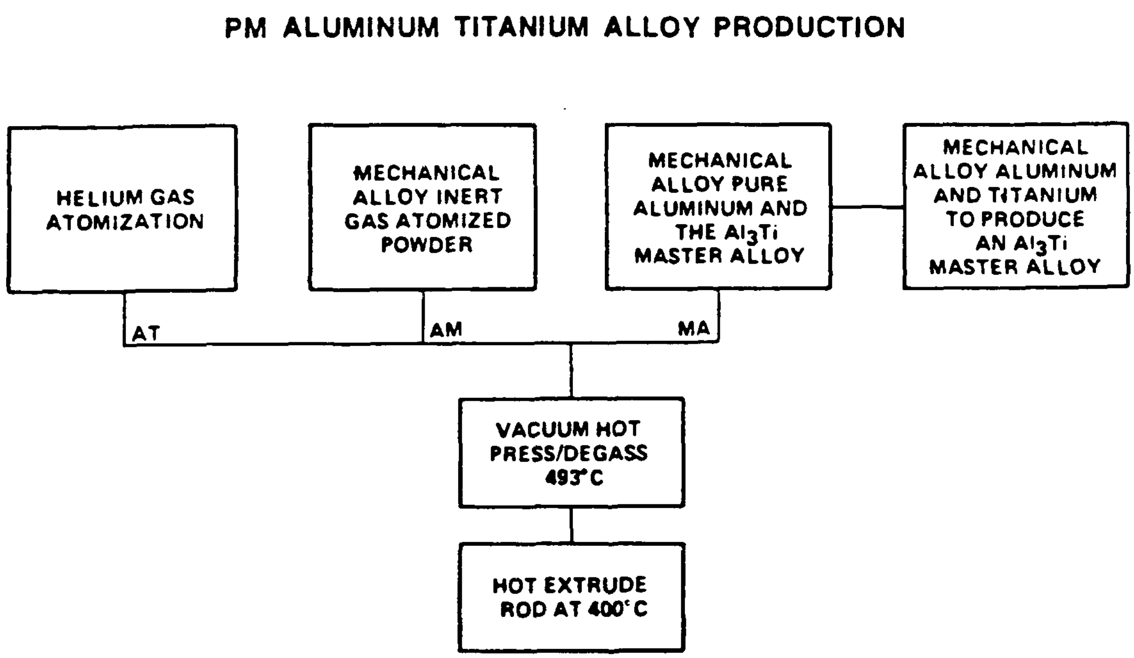

Fig. 3 Alloy Processing Scheme.

a

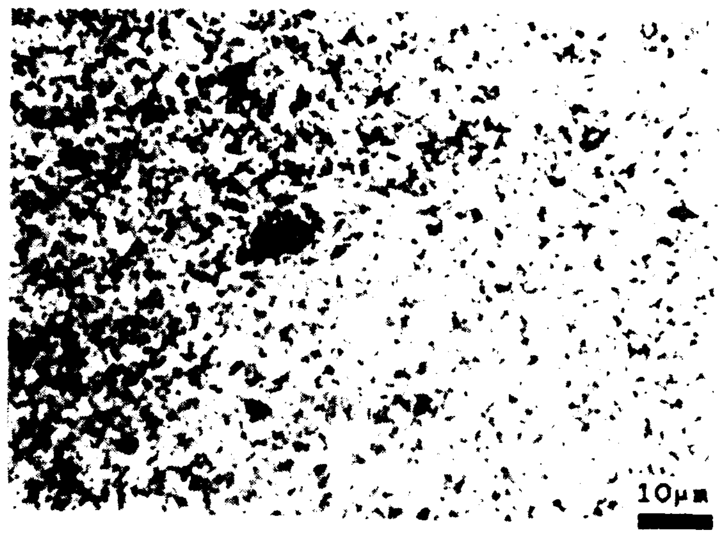

b

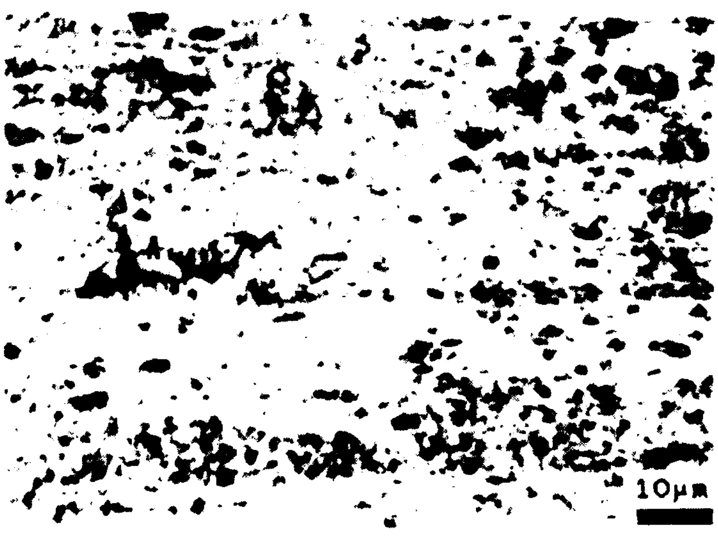

c

Fig. 4 Optical Micrographs of Alloy a) AT6, b) AM6, and c) MA6

a

b

c

Fig. 5 TEM Micrographs of a) AT6, b) AM6, and c) MA6

a

b

c

Fig.6 TEM Micrographs of Annealed a) AT6, b) AM6, and c) MA6

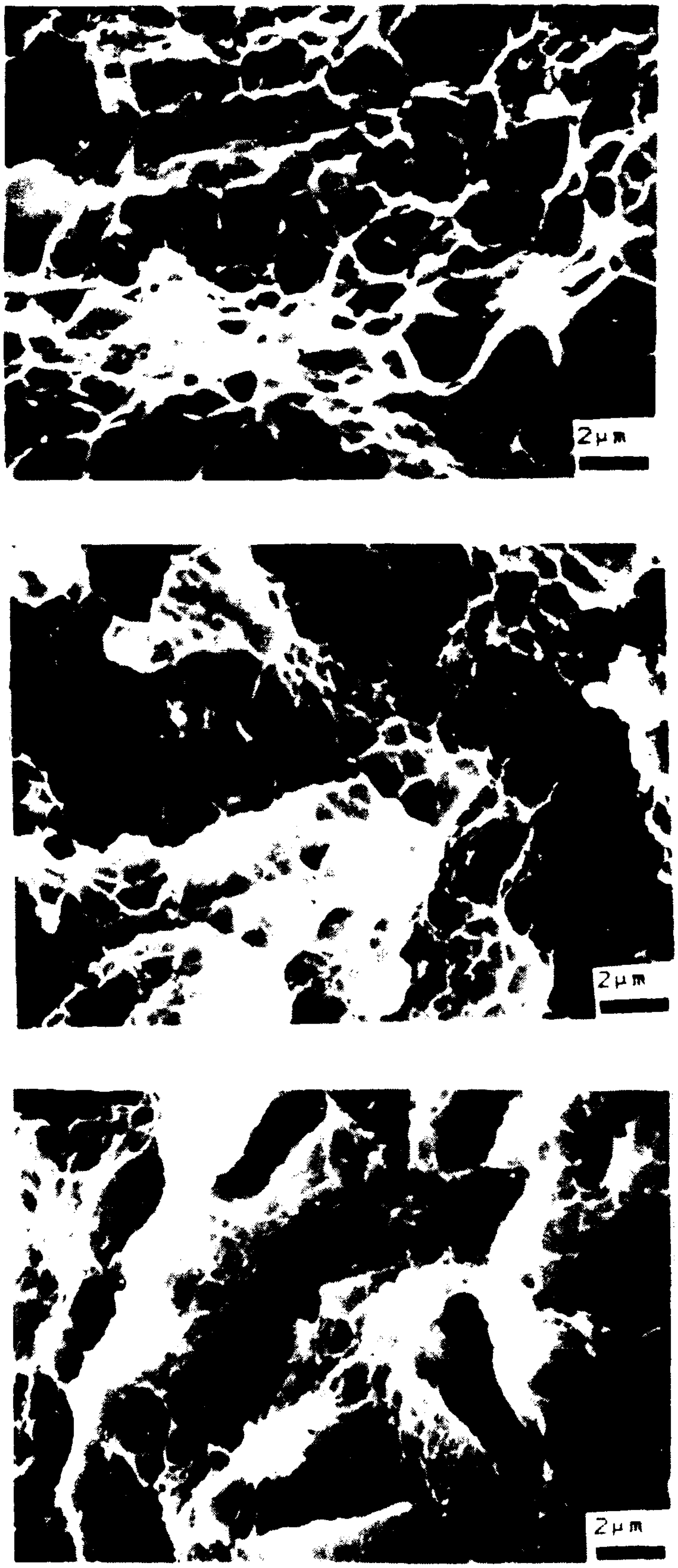

a

b

c

Fig. 7 SEM Tensile Fractographs of a) AT4, b) AM4, and c) MA4

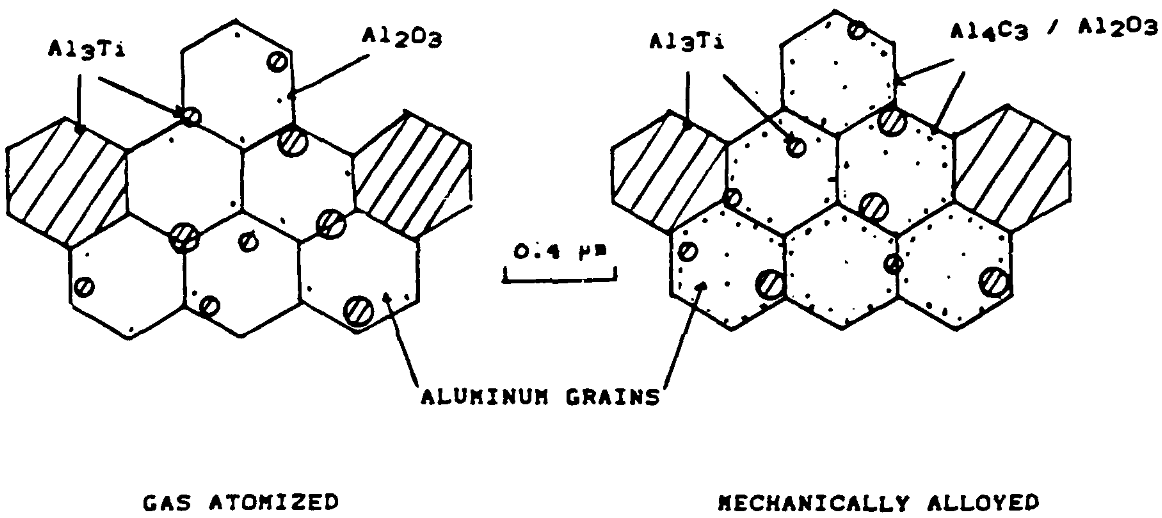

Fig. 8 Microstructural Model Illustrating the Relative Size and Spacing of Particles and Grains.

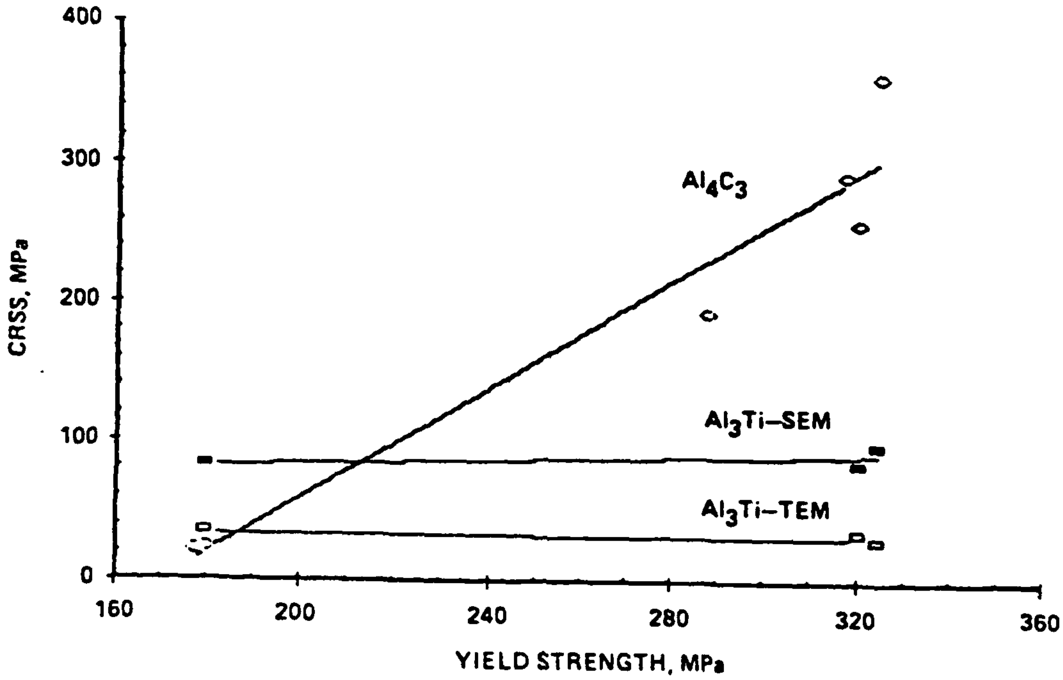

Fig. 9 Calculated Orowan Strengthening of Dispersoids Versus Alloy Strength.

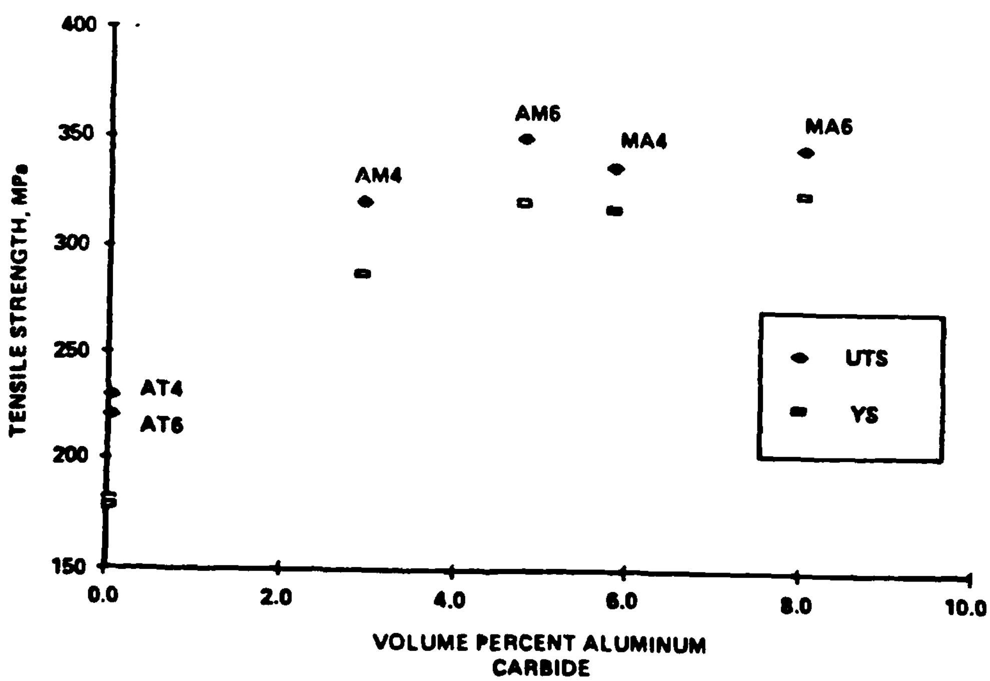

Fig. 10 Effect of Aluminum Carbides on Tensile Strength.

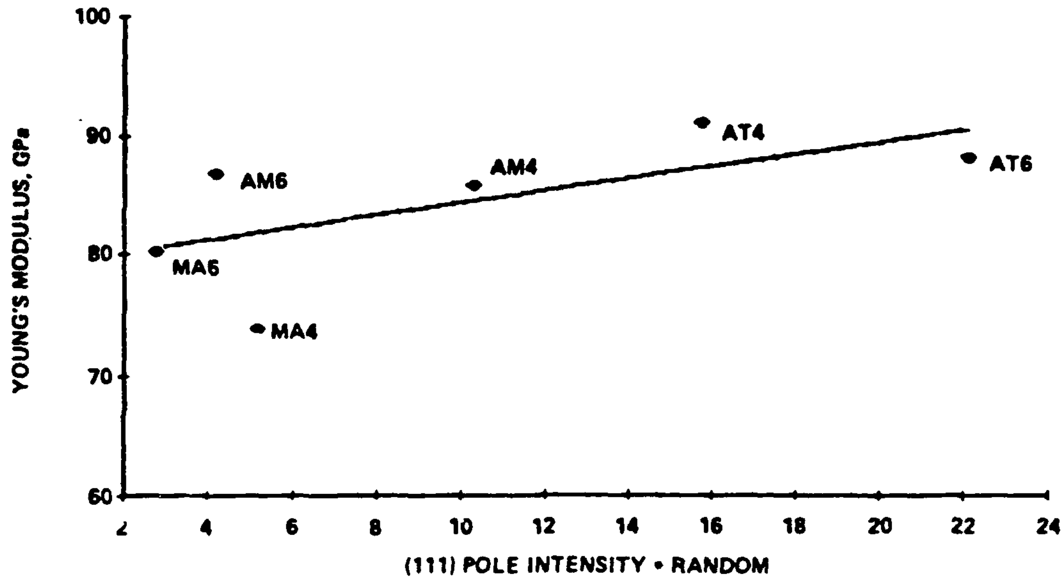

Fig. 11 Effect of Texture on Young's Modulus.

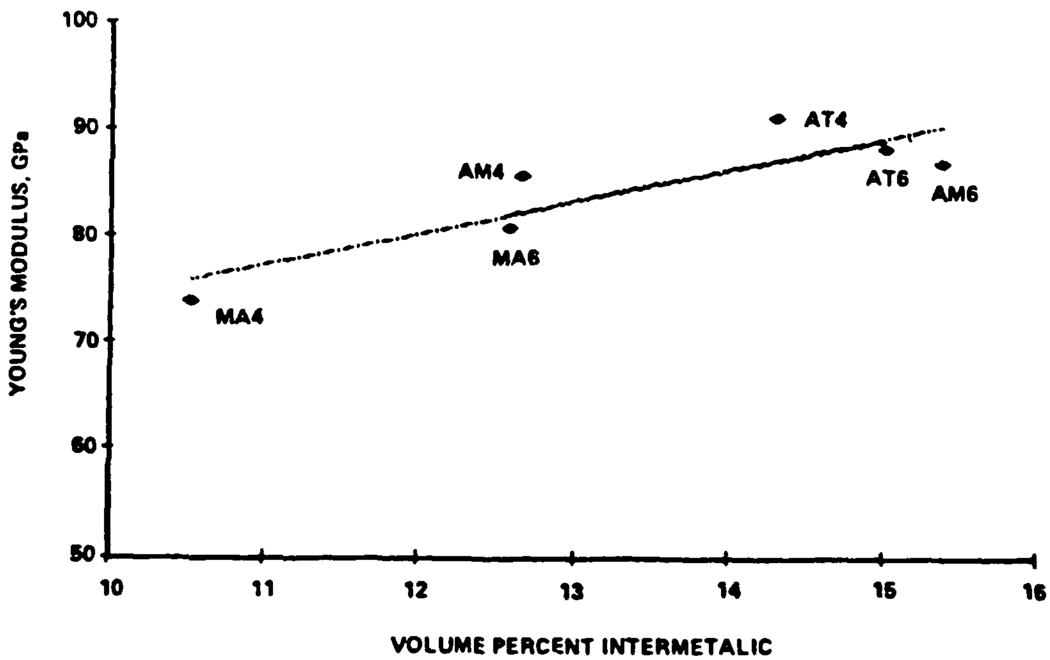

Fig. 12 Effect of Al_3Ti on Young's Modulus.

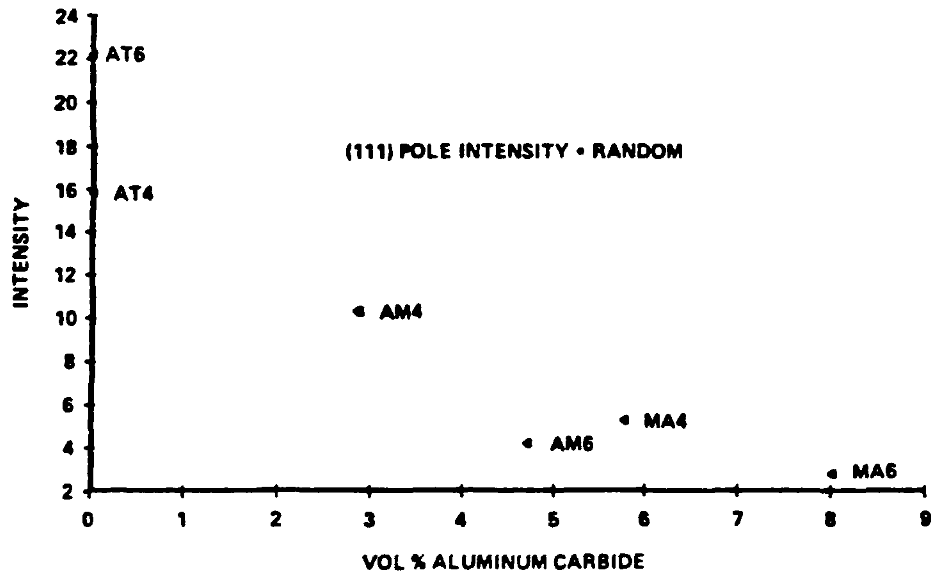

Fig. 13 Effect of Dispersoids on Texture Development.

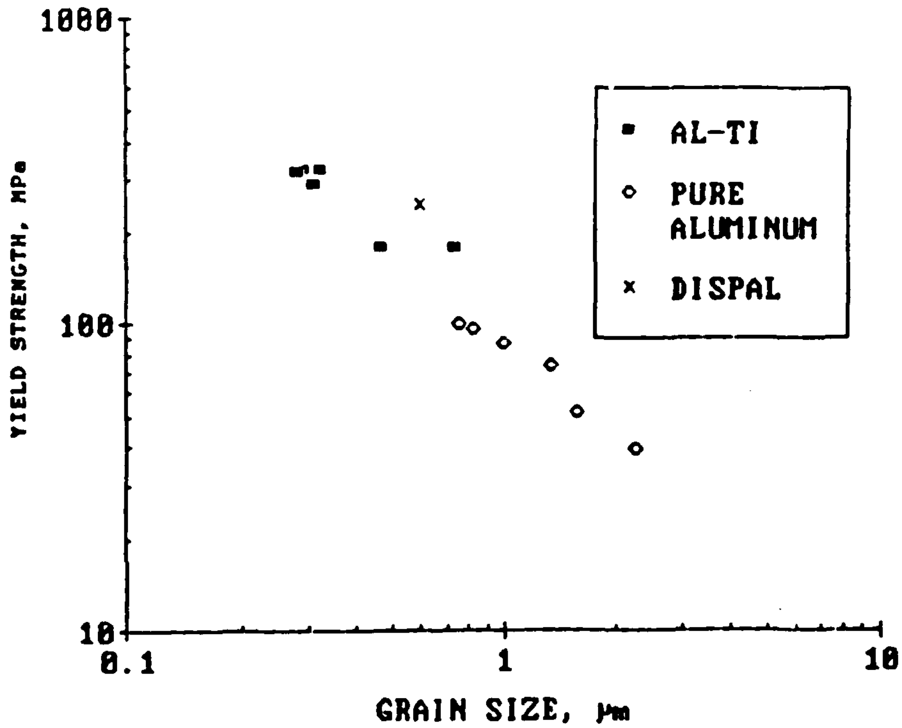

Fig. 14 Effect of Grain Size on Yield Strength.

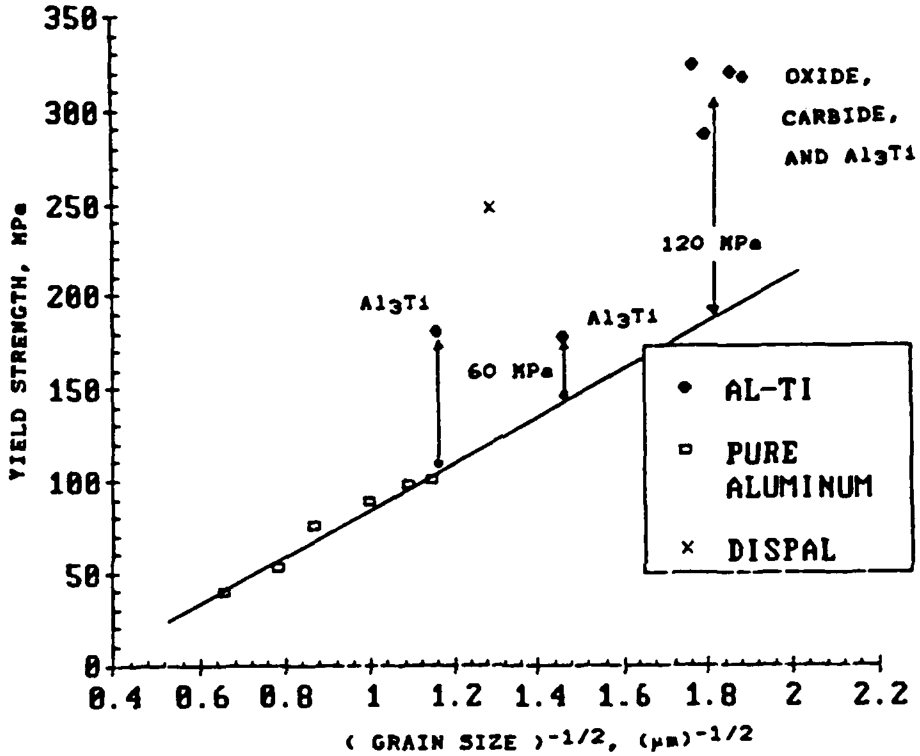

Fig. 15 Hall-Petch Plot of Pure Aluminum and the Aluminum Aluminum Titanium Alloys.

DISTRIBUTION LIST (Continued)

REPORT NO. NADC 88067-60

No. of Copies

National Science Foundation, Office of Science and
Technology Centers Division, 1800 G Street,
Washington, DC 20550 1

Office of Naval Research, Washington, DC 20350,
S. Fishman Code 431 1

Office of Naval Technology, Arlington VA,
J. Kelley OCNR-225 1

Rockwell International, Science Center, 1049 Camino Dos Rios,
P.O. Box 1085, Thousand Oaks, CA 91360 1

Sandia National Laboratory, Albuquerque, NM
87185, Div. 1822 and 1832 2

TRW, Inc., 23555 Euclid Ave., Cleveland, OH 44117 1

U.S. Army Air Mobility R&D Laboratory, Fort Eustis, VA
23064,SAVDL-EU-SS 1

United Technologies, Pratt and Whitney, P.O. Box 2691,
West Palm Beach, FL 33402, J. Simon, Jr. 1

USAF Systems Command,WPAFB, OH 45331 1

University of California, Dept. of Mechanical Engineering,
Irvine, CA 92717, E.J. Lavernia 1

University of Virginia, Light Metals Center,
Charlottesville, VA 22901,
J. Wert, J. Hawk, E.A. Starke, Jr. 3

NAVAIRDEVCEN, Library, Code 8131 (2 copies),
W.E. Frazier, Code 6063 (28 copies) 30

Center for Naval Analyses
4401 Font Ave., P.O.Box 16268
Alexandria, VA 22302-0268 1

Defense Technical Information Center (DTIC)
Bldg. #5, Cameron Station, Alexandria, VA 22314
(ATTN: Administrator) 2

DISTRIBUTION LIST (Continued)

REPORT NO. NADC 88067-60

	No. of Copies
Lockheed Missiles and Space Co., Metallurgy Dept. 93-10/204 3251 Hanover St., Palo Alto CA 94304, R. Lewis and J. Wadworth	2
Marko Materials Inc., 144 Rangeway Rd., N.Billerica, MA 01862, R. Ray	1
Martin Marietta Laboratories, 1450 South Rolling Rd., Baltimore, MD 21227-3898, J. Venables	1
Material Science Corporation, 1777 Walton Rd., Blue Bell, PA 19422	1
McDonnell Aircraft Co., Box 516, Saint Louis, MO 63166, V.M. Vasey-Glandon and K.K. Sankaran	2
MCIC, Battelle Memorial Institute, Columbus OH	1
Metcut-Materials Research Group, P.O. Box 33511, Wright Patterson AFB, OH 45433, Y.W. Kim	1
NASA Headquarters, 600 Independence Ave., Washington, DC 20546, Mr. N. Mayer	1
NASA Langley Research Center, Hampton, VA 23365, A. Taylor	1
National Bureau of Standards, Gaithersburg, MD 20899,J.R. Manning	1
NAVAVNDEP,MCAS, Cherry Point, NC Code 340	1
NAVAVNDEP, NAS Alameda, CA Code 340	1
NAVAVNDEP, NAS Jacksonville, FL Code 340	1
NAVAVNDEP, NAS Norfolk, VA Code 340	1
NAVAVNDEP, NAS North Island, CA Code 340	1
NAVAVNDEP, NAS Pensacola, FL Code 340	1
NAVAIRSYSCOM, Washington, DC 20361, J. Collins, Air-5304, L. Sloter Air 931	2
NAVAIRTESTCEN, Patuxent River, MD	1
Naval Air Propulsion Test Center, Trenton, NJ 08628, R. Mahortor	1
Naval Surface Weapons Center, Dahlgren, VA 22448-5000	1
Naval Surface Weapons Center, Silver Spring, MD 20903-5000, D. Divecha	1
Naval Post Graduate School, Mechanical Engineering Dept., Monterey, CA 93943	1
Naval Research Laboratory, Washington, DC 20375, Code 6120, Code 6306	2
Naval Ship Engineering Center, Washington, DC 20360, Code 6101E	1
NAVAVNSAFECEN, NAS Norfolk VA	1
NAVSEASYSCOM, Washington, DC 20362	1
NAVSHIPRANDCEN, Annapolis, MD 21402	1
NAVSHIPRANDCEN, Bethsesda, MD 20034	1
Northrop, Aircraft Division, One Northrop Ave., Hawthorne, CA 90250, S.P. Agrawal and G.R. Chanani	2

DISTRIBUTION LIST

REPORT NO. NADC 88067-60

	No. of Copies
Air force Wright Aeronautical Lab, Wright Patterson AFB, OH 45433, W. Griffith	1
Alcan Rolled Products Co, 100 Erieview Plaza, Cleveland, OH 44144, P. Wakeling	1
Alcoa, 1501 Alcoa Building, Pittsburgh, PA 15219, F.R. Billman and G.J. Hildeman	2
Allied Corp, P.O. Box 1021R, Morristown, NJ 07960 S.K. Das and P. Gilman	2
Army Materials and Mechanics Research Center, Watertown, MA	1
Avco Corp., Applied Technology Division, Lowell, MA 01851	1
Battelle Memorial Institute, Columbus Laboratories 505 King Av., Columbus, OH 43201	1
Boeing Commercial Airplane, Seattle, WA, W. Quist	1
Boeing Corp., Aerospace Division, P.O. Box 3707, Seattle, WA 98124	1
Boeing-Vertol Co., P.O. Box 16858, Phila, PA 19142, Dept. 1951	1
British Alcan Aluminum Ltd., Alcan International, Southam Rd., Bamburt, Orfordshire OX 167Sp, United Kingdom, R. Grines	1
Brookhaven National Laboratory, Department of Applied Science/PSD, Building 526, Upton, NY 11973	1
Clemson University, Dept. of Mechanical Engineering, Riggs Hall, Clemson, SC 29634-0921, H.J. Rack	1
DARPA, 1400 Wilson Blvd., Arlington, VA 22209, B. Wilcox	1
Defense Technical Information Center, Cameron Station, Bldg. 5, Alexandria, VA 22314	12
Department of Energy, 100 Independence Ave., SW Washington, DC 20585, Code CE142	1
Drexel University, Dept. of Materials Engineering, 32nd and Chestnut St., Phila., PA 19104, M.J. Koczak	1
General Dynamics, Convair Aerospace Division, P.O. Box 748, Fort Worth, TX 76101, Tch. Library	1
General Electric Co., Valley Forge Space Center, Phila., Pa 19101	1
Grumman Aerospace Corp., Bethpage, NY 11714, PN Adler	1
Inco Alloys International, P.O. Box 1958, Huntington, WV 25720, R. Schelleng and R. Benn	2
Innovare Inc., Ben Franklin Technology Center, South Mountain Dr., Bethlehem, PA 18015 A.R. Austen	1
Kaiser Aluminum, Ravenswood works, Ravenwood, WV 26164 J.M. Hunter	1
Lockheed California Co., Burbank, CA 9152-7631, D.J. Chellman	1